Basic Study on Range Extension Autonomous Driving of Electric Vehicle Considering Velocity Constraint for Real-Time Implementation

Takuya Fukuda[*a)] Student Member, Hiroshi Fujimoto[*] Senior Member
Yoichi Hori[*] Fellow, Daisuke Kawano[**] Non-member
Yuichi Goto[**] Non-member, Yusuke Takeda[***] Non-member
Koji Sato[***] Non-member

Nowadays Electric Vehicles (EVs) attract people's attention as means of preventing global warming that depends on the artificial factor like increase of CO_2 emissions. However, EVs need to be improved the problem of their short cruising range to spread around people. This paper proposes two method with short calculation time for real-time optimization to extend cruising range from the point of view of Range Extension Autonomous Driving. One is the method of using analytical solution with approximation model, the other is one of using dynamic programming. The effectiveness of the proposed method is verified by simulations and experimen

Keywords: Electric Vehicle, Optimization, Range Extension Autonomous Driving, Velocity Constraint

1. Introduction

The climate change caused by artificial factor like global warming is considered a social problem these days. As means of alleviating the effect, Electric Vehicles (EVs) using electric motor instead of internal combustion engines (ICEs) catch the great people's attention. Compared with ICEs vehicle, EVs have many advantages thanks to motors [1].

(1) Torque generation of a motor is much faster than that of an engine (several milliseconds vs. several hundred milliseconds).
(2) Motor torque can be estimated precisely from the current.
(3) For EVs with in-wheel motors, each wheel can be controlled independently.
(4) Motors not only can be used for driving, but also for regenerative braking.

On the other hand, there is a disadvantage that EVs have short cruising range. Especially for consumers, long cruising range is one of great factors that motivate them to purchase a EV [2], so that range improvement is a large problem to be solved and many research has been conducted in this field. For instance, new power train that includes Snubber Assisted Zero voltage Zero current transition (SAZZ) chopper between the battery and the inverter to control dc link voltage is proposed to reduce energy consumption from the viewpoint of EVs' hardware [3]. In addition, wireless power transfer to the EVs' body while driving [4]~[6], and proposing simple magnetic circuit of IPMSM using permeance method to minimize energy loss through design of motor parameters [7] have also been researched. From viewpoint of softwares, there are researches for range extension by considering stop and go of EVs to generate optimal velocity trajectory [8], by considering signal information and traffic congestion due to the signal to generate optimal velocity trajectory [9][10], by searching optimal route [11], by optimally distributing driving force [12][13], and by simultaneously optimizing the speed trajectory generation and driving force distribution [14][15].

Optimization for reducing power consumption of EVs requires long computation time, so research performing offline calculation is current mainstream. However, in actual traveling, there are many cases where it is not possible to travel as obtained optimum solution due to various external factors such as congestion, construction, accident, etc. so it is desirable to calculate in real time. Therefore, in this paper, two methods of a Range Extension Autonomous Driving (READ) that satisfies the velocity constraint in a certain section are proposed by using a short calculation time optimization method with a view to calculate online in the future. One is the method of using analytical solution with approximation model, the other is one of using dynamic programming. The reminder of this paper is organized as follows. Experimental vehicle with four in-wheel motor is shown and modeled in the second section. Two optimization methods with short calculation time are proposed in the third and fourth section. Simulation and experiment results are shown and the effectiveness of the proposed methods is verified in the fifth section. The conclusion of this paper is drawn in the sixth section.

2. Vehicle Model

Fig.1 shows experimental vehicle, FPEV2-Kanon, manufactured by authors research group. The feature of this vehicle is that it has four in-wheel motor which can be controlled

a) Correspondence to: fukuda16@hflab.k.u-tokyo.ac.jp
[*] The University of Tokyo, 5-1-5 Kashiwanoha, Kashiwa, Chiba, 277-8561 Japan
[**] National Traffic Safety and Environment Laboratory, 7-42-27, Jindaijihigashimachi, Chofu, Tokyo, 182-0012 Japan
[***] Ono Sokki Co.,Ltd., 3-9-3, Shin-Yokohama, Kohoku-ku, Yokohama, Kanagawa, 222-8507 Japan

Fig. 1. FPEV2-Kanon.

Table 1. Vehicle Specification.

Vehicle mass M	854 kg
Wheelbase l	1.715 m
Distance from the center of gravity to the front and rear axles l_f,l_r	l_f:1.013 m l_r:0.702 m
Height of the center of gravity h_g	0.51 m
Front wheel inertia J_{ω_f}	1.24 kg·m^2
Rear wheel inertia J_{ω_r}	1.26 kg·m^2
Wheel radius r	0.302 m

independently. Vehicle specifications are shown Tab.1.

2.1 Vehicle Longitudinal Dynamic Model When considering straight driving, left and right motors generate the same amount of torque. In addition, torque is equally distributed to front and rear motors. The rotational motion equation of each wheel, the vehicle equation of motion, and total braking / driving force are given as

$$J_{\omega_j}\dot{\omega}_j = T_j - rF_j, \quad (1)$$

$$M\dot{V} = F_{\mathrm{all}} - \mathrm{sgn}(V)F_{\mathrm{DR}}, \quad (2)$$

$$F_j = \frac{1}{4}F_{\mathrm{all}}, \quad (3)$$

where j is the subscript of each wheel, J_{ω_j} is the wheel inertia, ω_j is the wheel angular velocity, T_j is the motor torque, r is the wheel radius, F_j is the braking / driving force, M is the vehicle mass, V is the vehicle velocity, sgn(V) is the signum function and if $V > 0$, it equals one, otherwise it equals zero. Here F_{DR} is the driving resistance and expressed as

$$F_{\mathrm{DR}}(V) = \mu_0 Mg + b|V| + \frac{1}{2}\rho C_d A V^2, \quad (4)$$

where μ_0 is the rolling friction coefficient, b is the factor proportional to V, ρ is the air density, C_d is the drag coefficient, and A is frontal projected area.

2.2 Tyre Model The slip ratio λ_j is given as

$$\lambda_j = \frac{V_{\omega_j} - V}{\max(V_{\omega_j}, V, \epsilon)}, \quad (5)$$

where V_{ω_j} is the wheel velocity and ϵ is a positive constant close to zero to avoid division by zero. It is known that the slip ratio λ is related with the friction coefficient μ as shown in Fig.2. In the region of $|\lambda| << 1$, μ is nearly proportional to λ. Define the driving stiffness $D_s{}'$ as the slope of the curve, the braking/driving force of each wheel is given as

$$F_j = \mu_j N_j \simeq D_s{}' N_j \lambda_j, \quad (6)$$

where N_j is the normal force of each wheel. When driving at V and F_{all}, N_f and N_r are respectively calculated as

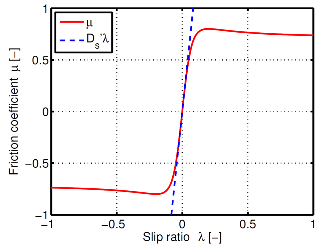

Fig. 2. μ-λ Curve.

$$N_f(V, F_{\mathrm{all}}) = \frac{1}{2}\left[\frac{l_r}{l}Mg - \frac{h_g}{l}\{F_{\mathrm{all}} - \mathrm{sgn}(V)F_{\mathrm{DR}}(V)\}\right], \quad (7)$$

$$N_r(V, F_{\mathrm{all}}) = \frac{1}{2}\left[\frac{l_f}{l}Mg + \frac{h_g}{l}\{F_{\mathrm{all}} - \mathrm{sgn}(V)F_{\mathrm{DR}}(V)\}\right], \quad (8)$$

where l_f and l_r are respectively the distance from the center of gravity to front and rear axles, l is the wheelbase, and h_g is the height of the center of gravity.

2.3 Inverter Input Power Model In this subsection, the inverter input power is modeled. Neglecting the mechanical loss of the motor and the inverter loss, the inverter input power P_{in} is described as

$$P_{\mathrm{in}} = P_{\mathrm{out}} + P_{\mathrm{c}} + P_{\mathrm{i}}, \quad (9)$$

where P_{out} is the sum of the mechanical outputs of each motor, P_{c} is the sum of the copper losses of each motor, and P_{i} is the sum of the iron losses of each motor [16].

Suppose that the torque caused by the wheel inertia and slip ratio λ_j are small enough. Then the motor torque T_j and the wheel angular velocity ω_j are given as

$$T_j \simeq rF_j, \quad (10)$$

$$\omega_j \simeq \frac{V}{r}(1 + \lambda_j). \quad (11)$$

Therefore P_{out} is calculated as

$$P_{\mathrm{out}} = 2\sum_{j=f,r}\omega_j T_j \simeq \frac{1}{2}VF_{\mathrm{all}}\sum_{j=f,r}\left(1 + \frac{F_{\mathrm{all}}}{4D_s{}'N_j(V, F_{\mathrm{all}})}\right). \quad (12)$$

In the modeling of the copper loss P_{c}, the iron loss resistance is neglected for simplicity. Suppose that the magnet torque and the q-axis current are much larger than the reluctance torque and the d-axis current, respectively. Then, the sum of the copper losses P_{c} is given as

$$P_{\mathrm{c}} = 2\sum_{j=f,r}R_j {i_{qj}}^2 \simeq \frac{r^2}{8}{F_{\mathrm{all}}}^2\sum_{j=f,r}\frac{R_j}{{K_{tj}}^2}, \quad (13)$$

where R_j is the armature winding resistance of the motor, i_{qj} is the q-axis current, and K_{tj} is the torque coefficient of the motor. Next, the iron loss is modeled. In this paper, based on the well-known equivalent circuit model. Fig.3 shows the d and q-axis equivalent circuits of the permanent magnetic synchronous motor. From Fig.3, the sum of the iron losses P_{i}

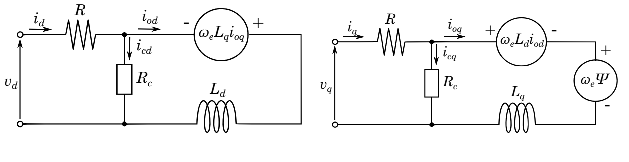

(a) d-axis. (b) q-axis.

Fig. 3. Equivalent Circuit of PMSM.

is expressed as

$$\begin{aligned}P_{\mathrm{i}} &= 2\sum_{j=f,r}\frac{{v_{odj}}^2+{v_{oqj}}^2}{R_{\mathrm{c}j}}\\ &= 2\sum_{j=f,r}\frac{{\omega_{\mathrm{e}j}}^2}{R_{\mathrm{c}j}}\left\{\left(L_{dj}i_{odj}+\Psi_j\right)^2+\left(L_{qj}i_{oqj}\right)^2\right\}\\ &\simeq 2\frac{V^2}{r^2}\sum_{j=f,r}\frac{{P_{\mathrm{n}j}}^2}{R_{\mathrm{c}j}}\left\{\left(\frac{rL_{qj}F_{\mathrm{all}}}{4K_{\mathrm{t}j}}\right)^2+{\Psi_j}^2\right\},\cdots\cdots\ (14)\end{aligned}$$

where v_{odj} and v_{oqj} are respectively the d and q-axis induced voltages, R_{cj} is the equivalent iron loss resistance, ω_{ej} is the electrical angular velocity of each motor, L_{dj} is the d-axis inductance, L_{qj} is the q-axis inductance, i_{odj} and i_{oqj} are respectively the differences between the d and q-axis currents and the d and q-axis components of the iron loss current, $P_{\mathrm{n}j}$ is the number of pole pairs, and Ψ_j is the interlinkage magnetic flux. The equivalent iron loss resistance R_{cj} is described as

$$\frac{1}{R_{\mathrm{c}j}(\omega_{\mathrm{e}j})}=\frac{1}{R_{\mathrm{c}0j}}+\frac{1}{R_{\mathrm{c}1j}'|\omega_{\mathrm{e}j}|}.\cdots\cdots\cdots\cdots\ (15)$$

In (15), the first and second terms of right hand side are respectively the eddy current loss and the hysteresis loss.

3. Range Extension Autonomous Driving Considering Velocity Constraint with Approximation Model

Total driving section is divided into the section with and without velocity constraint to consider it as shown in Fig.4. Optimization problem is given as

$$\min \quad W_{in}=\int_{t_0}^{t_2}P_{in}(k,V,\dot{V})dt,\quad\cdots\ (16)$$

subject to :

$$\int_{t_0}^{t_1}V(t)dt=X_1,\ \int_{t_1}^{t_2}V(t)dt=X_2,\cdots\ (17)$$

$$V(t_0)=V_0,\ V(t_2)=V_2,\quad\cdots\ (18)$$

$$V(t)\le V_c,\ \text{ for } t_1\le t\le t_2,\quad\cdots\ (19)$$

where t_0 is the initial time, t_1 is the time when EVs enter the section 2 with velocity constraint, t_2 is the final time, X_1 is the travel distance for section 1, X_2 is the travel distance for section 2, V_0 and V_2 are the boundary conditions, and V_c is the maximum of velocity constraint. Two methods are proposed to solve this problem. One is using analytical solution with approximation model, the other is using dynamic programming. Approximation model is introduced below.

3.1 Approximation Model Optimization problem without velocity constraint is given as

$$\min\ W_{in}=\int_{t_0}^{t_2}P_{in}(V,\dot{V})dt,\ \cdots\cdots\cdots\ (20)$$

subject to :

$$\int_{t_0}^{t_2}V(t)dt=X_1+X_2,\ \cdots\cdots\cdots\ (21)$$

$$V(t_0)=V_0,\ V(t_2)=V_2.\cdots\cdots\cdots\ (22)$$

To obtain analytical solution, an approximation model [15] for this problem is used. An approximation model ignores the inverter loss, motor iron loss, mechanical loss and slip ratio, and approximates driving resistance up to the first degree. The inverter input power P_{in} is expressed as

$$\begin{aligned}P_{\mathrm{in}}(V,\dot{V}) \sim\ & a_{20}\dot{V}^2+a_{11}\dot{V}V+a_{10}\dot{V}+a_2V^2\\ &+a_1V+a_0.\cdots\cdots\cdots\cdots\ (23)\end{aligned}$$

Here,

$$\left\{\begin{array}{ll}a_{20} & =\frac{2R_f}{{K_{tf}}^2}\left\{\frac{J_{\omega f}}{r}+\frac{Mr}{4}\right\}^2+\frac{2R_r}{{K_{tr}}^2}\left(\frac{J_{\omega r}}{r}+\frac{Mr}{4}\right)^2\\ a_{11} & =M+\frac{2}{r^2}(J_{\omega_f}+J_{\omega_r})+\frac{bR_r}{{K_{tr}}^2}\left(J_{\omega_r}+\frac{Mr^2}{4}\right)\\ & \quad+\frac{bR_f}{{K_{tf}}^2}\left\{J_{\omega_f}+\frac{Mr^2}{4}\right\}\\ a_{10} & =\frac{\mu_0MgR_r}{K_{tr}^2}\left(J_{\omega_r}+\frac{Mr^2}{4}\right)+\frac{\mu_0MgR_f}{{K_{tf}}^2}\left\{J_{\omega_f}+\frac{Mr^2}{4}\right\}\\ a_2 & =b+\frac{b^2r^2}{4}\left\{\frac{R_f}{4{K_{tf}}^2}+\frac{R_r}{4{K_{tr}}^2}\right\}\\ a_1 & =\mu_0Mg+\frac{\mu_0^2M^2g^2br^2}{2}\left\{\frac{R_f}{4{K_{tf}}^2}+\frac{R_r}{4{K_{tr}}^2}\right\}\\ a_0 & =\frac{\mu_0^2M^2g^2r^2}{2}\left\{\frac{R_f}{4{K_{tf}}^2}+\frac{R_r}{4{K_{tr}}^2}\right\}\end{array}\right.\ (24)$$

The velocity trajectory V which is a solution to this problem is obtained by solving the Euler Lagrangian equation given as

$$\begin{aligned}&\frac{d}{dt}\left(\frac{\partial P_{\mathrm{in}}(V,\dot{V})}{\partial\dot{V}}\right)-\frac{\partial P_{\mathrm{in}}(V,\dot{V})}{\partial V}\\ &\quad+\lambda\left\{\frac{d}{dt}\left(\frac{\partial V}{\partial\dot{V}}\right)-\frac{\partial V}{\partial V}\right\}=0,\cdots\cdots\cdots\ (25)\end{aligned}$$

where λ is Lagrangian multiplier. From (25), the differential equation is given as

$$2a_{20}\ddot{V}-2a_2V=a_1+\lambda.\cdots\cdots\cdots\ (26)$$

By solving (26), optimal velocity trajectory V is given as

$$V(t)=A_1e^{\alpha t}+B_1e^{-\alpha t}+\beta.\cdots\cdots\cdots\ (27)$$

Here,

$$\alpha=\sqrt{\frac{a_2}{a_{20}}},\ \cdots\cdots\cdots\ (28)$$

$$\beta=-\frac{a_1+\lambda}{2a_2}.\cdots\cdots\cdots\ (29)$$

The integral constants A_1 and B_1 are determined to satisfy the boundary conditions and (21).

3.2 Optimization Problems with Velocity Constraint by Approximation Model In the previous subsection, the velocity trajectory was obtained over the entire section. On the other hand, to derive the velocity trajectory that satisfies the constraint, the analytical solution is separately derived in section 1 and section 2 which have a common boundary condition V_1 that satisfies the velocity constraint, so that the entire velocity trajectory is obtained as shown in Fig.4.

There are three variables to consider for W_{in} minimization

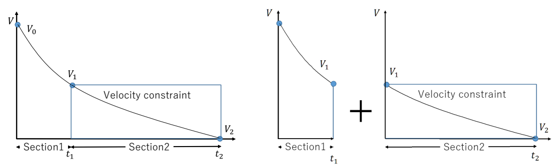

(a) Total Traveling Section. (b) Divided Section.

Fig. 4. Division of Traveling Section.

in Fig.4.

(1) The common boundary condition velocity V_1.

(2) The time when EV entering the section 2 t_1.

(3) The final time t_2.

In this case, V_1, t_1, and t_2 are regarded as variables. The velocity trajectory also consists of these variables because (27) is uniquely determined by the boundary conditions.

Consumption energy in each section is given as

$$W_{in1} = \int_0^{t_1-t_0} P_{in}(V, \dot{V})dt \,|_{V=V_{\text{section1}}(t)}, \quad \cdots\cdots\cdots (30)$$

$$W_{in2} = \int_0^{t_2-t_1} P_{in}(V, \dot{V})dt \,|_{V=V_{\text{section2}}(t)}, \quad \cdots\cdots\cdots (31)$$

$$W_{in} = W_{in1} + W_{in2}, \cdots\cdots\cdots (32)$$

where W_{in1} (W_{in2}) and $V_{\text{section1}}(t)$ ($V_{\text{section2}}(t)$) are the consumption energy and velocity trajectory in the section 1 (section 2) respectively. Since the initial and the final velocity are supposed to be given, W_{in1} (W_{in2}) and $V_{\text{section1}}(t)$ ($V_{\text{section2}}(t)$) can be expressed as variables of V_1 and $t_1(t_2)$ respectively.

W_{in} is a downwardly convex quadratic function with respect to V_1. V_{1opt} which minimizes W_{in} is given as follows by solving for V_1.

$$\frac{\partial W_{in}}{\partial V_1} = 0. \cdots\cdots\cdots (33)$$

If this V_{1opt} is less than or equal to the velocity constraint, the value is used as it is. However, depending on the condition, the value may exceed the velocity constraint. In that case, since W_{in} is a downwardly convex quadratic function for V_1, V_{1opt} which gives the minimum W_{in} and satisfies the velocity constraint is given as

$$V_{opt}(t_1) = V_c, \cdots\cdots\cdots (34)$$

where V_c is the maximum value of the velocity constraint. Next, consider t_1 and t_2. It is impossible to obtain analytical solutions of V_{1opt} and W_{in} which is the minimum for t_1 and t_2 because they are exponential functions consisting of complicated terms for t_1 and t_2. Therefore, V_{1opt} and minimum W_{in} are searched for t_1 and t_2 given as

$$0 \leq t_1 \leq \frac{4X_1}{V_0 + V_c}, \cdots\cdots\cdots (35)$$

$$0 \leq t_2 \leq \frac{4X_2}{V_2 + V_c}. \cdots\cdots\cdots (36)$$

That is, t_1 and t_2 are searched within a range twice the time required for constant deceleration. Here, the sampling interval is 0.01 second. From the above, when the velocity constraint is satisfied, it is possible to derive the optimal velocity trajectory with velocity constraint in the case of using the approximation model by finding the optimal boundary conditions V_1, t_1, and t_2 .

4. Range Extension Autonomous Driving Considering Velocity Constraint with Detailed Model

In order to obtain an global optimal solution of the deceleration trajectory considering the velocity constraint with detailed model, dynamic programming used for the calculation of the velocity trajectory in the railway field [17] is employed. Dynamic programming is the method of practical full search of time, speed, and distance, so it always has the feature that global optimal solution can be obtained. However, traveling time is regarded as a free parameter to reduce computation cost in this study by introducing discrete time-distance transformation given below so that three-dimensional search becomes two-dimensional search.

$$\Delta x = \frac{V(m) + V(m+1)}{2}\Delta t, \cdots\cdots\cdots (37)$$

where Δx is a constant distance and Δt is a variable traveling time between adjacent node, and $V(m)$ is a velocity at the position $m\Delta x$. Therefore, optimization problem is given as

$$\min W_{in} = \textstyle\sum_{m=1}^{N-1} P_{in}\left(\frac{V(m)+V(m+1)}{2}, \frac{V(m)^2-V(m+1)^2}{2\Delta x}\right) \times \frac{2\Delta x}{V(k)+V(k+1)}, \quad (38)$$

subject to :

$$\textstyle\sum_{m=1}^{N-1} \Delta x = X_1 + X_2, \quad (39)$$

$$V(0) = V_0, \; V(N) = V_2. \quad (40)$$

$$V(m) \leq V_c, \text{ for } l \leq m \leq N, \quad (41)$$

where $l\Delta x$ is the position at beginning velocity constraint.

The algorithm of dynamic programming is as follows.

(1) The state space of position and velocity is divided for each Δx and Δv.

(2) Solve the equation of motion with respect to each node in m row from one in $m-1$ row, determine the velocity at position Δx, and also obtain the partial evaluation value (consumption energy during Δx) at that time.

(3) Find the sum of the evaluation value $J(\cdot, M)$ at the node in the m row and the partial evaluation value obtained in (2).

(4) If the evaluation value does not correspond to the velocity constraint, the smallest evaluation value and the velocity at that time are saved, and if the evaluation value corresponds to the velocity constraint, the evaluation value is ∞.

(5) Select the node backward from the last column so that the evaluation value becomes the minimum.

(6) The optimal velocity trajectory is obtained by starting the search from the initial point.

In actual driving, thanks to precomputation, it is possible to omit the backward search (1–5) and to start the derivation of the optimum velocity trajectory from the forward search of (6) by storing the optimal velocity and the evaluation value locally as a table. Therefore, it is a very powerful method

Table 2. Boundary Condition.

Travel distance $X_1 + X_2$	40 m
Travel distance w/o velocity constraint X_1	20 m
Initial velocity V_0	30 km/h
Velocity constraint V_1	15 km/h
Final velocity V_2	0 km/h

Table 3. Computation Time.

	Prop. 1	Prop. 2
Computation time	0.279 s	0.0647 s

in the case where precomputation is possible. In this case, the aim is to solve the optimum deceleration trajectory with no gradient and turning, the equation of motion for a neighboring node sequence from a certain point becomes equal in every row. Therefore, in order to reduce the calculation cost of precomputation, the equation of motion in (2) is not solved over the entire state space but is solved only in two adjacent node rows.

5. Simulations and Experiments

In this section, simulation and experimental results are shown. Conventional, proposed 1 and proposed 2 method respectively correspond to constant deceleration, analytical solution for approximation model, and dynamic programming. The simulation and experimental conditions are shown in Tab.2.

5.1 Simulations Fig.5 shows that the simulation result of regenerative energy is 22.29 kWs in case of conventional method, 22.50 kWs in case of proposed 1 method, and 22.54 kWs in case of proposed method 2. Regenerative energy increases 0.94% in method 1 and 1.1% in method 2 compared with conventional method. Tab.3 shows the computation time of simulation. Proposed methods have low computation cost.

5.2 Experiments of Field Test Experiments are conducted under the same condition as simulations. Fig.6 shows that the experimental result of regenerative energy is 21.68 kWs in case of conventional method, 23.08 kWs in case of proposed 1 method, 23.46 kWs in case of proposed method 2. Experimental results are similar to tendency of simulation ones. Regenerative energy increases 6.5% in method 1 and 8.2% in method 2 compared with conventional method.

5.3 Experiments of Real Car Simulation Bench Bench tests are also conducted under the same condition as simulations by using Real Car Simulation Bench (RC-S) [18] which belongs to Ono Sokki Co., Ltd. Fig.7 shows that the regenerative energy result of RC-S is 22.04 kWs in case of conventional method, 23.05 kWs in case of proposed 1 method, and 23.21 kWs in case of proposed method 2. Experimental results of bench test are similar to tendency of simulation and experimental ones. Regenerative energy increases 4.5% in method 1 and 5.3% in method 2 compared with conventional method.

6. Conclusion

Range Extension Autonomous Driving considering the velocity constraint is proposed. Since the analytical solution using the approximation model ignores various items as described in section 3, the velocity trajectory that truly minimizes the consumption energy is not obtained. Therefore, the proposed method 2, dynamic programming, which gives global optimal solution is used. Proposed method 1 and 2 increase the regenerative energy by 6.5% and 8.2% respectively in the field test. In addition, bench tests are also conducted and verified the effectiveness.

Both of two proposed methods have very short computation time, so they are suitable for real-time implementation.

As a future works, there may be mentioned optimization assuming that the velocity constraint changes during driving.

Acknowledgment

This research was partly supported by Industrial Technology Research Grant Program from New Energy and Industrial Technology Development Organization (NEDO) of Japan (number 05A48701d), the Ministry of Education, Culture, Sports, Science and Technology grant (number 22246057 and 26249061), and the Core Research for Evolutional Science and Technology, Japan Science and Technology Agency (JST-CREST). This result is a part of work in the project team of JST-CREST named "Integrated Design of Local EMSs and their Aggregation Scenario Considering Energy Consumption Behaviors and Cooperative Use of Decentralized In-Vehicle Batteries."

References

(1) Y. Hori: "Future Vehicle Driven by Electricity and Control - Research on Four-Wheel-Motored "UOT Electric March II"", IEEE Trans. on Industrial Electronics, Vol. 51, No. 5, pp. 954–962 (2004).

(2) Y. Tsuchiya, F. Ito, N. Tagashira, K. Baba, and T. Ikeya: "Analysis of Purchase Preferences for Electric Vehicles and Its Determinant Factors", CSIS Discussion Paper, No. 129, pp. 1–19 (2014) (in Japanese).

(3) M. Takeda, N. Motoi, G. Guidi, Y. Tsuruta, and A. Kawamura: "Driving Range Extension by Series Chopper Power Train of EV with Optimized de Voltage Profile", 38th Annual Conference on IEEE Industrial Electronics Society, Vol. 9, No. 18, pp. 2936–2941 (2012).

(4) J. Shin, S. Shin, Y. Kim, S. Ahn, S. Lee, G. Jung, S. Jeon, and D. Cho: "Design and Implementation of Shaped Magnetic-Resonance-Based Wireless Power Transfer System for Roadway-Powered Moving Electric Vehicles", IEEE Trans. on Industrial Electronics, Vol. 61, No. 3, pp. 1179–1192 (2014).

(5) T. E. Stamati and P. Bauer: "On-road Charging of Electric Vehicles", Transportation Electrification Conference and Expo, Vol. 15, No. 2, pp. 1–8 (2013).

(6) K. K. Ean, T. Imura, and Y. Hori: "New Wireless Power Transfer via Magnetic Resonant Coupling for Charging Moving Electric Vehicle," EVTeC & APE Japan 2014, pp. N/A (2014).

(7) D. Sato and J. Itoh: "Loss Minimization Design Using Permeance Method for Interior Permanent Magnet Synchronous Motor", IEEJ Trans. on Industry Applications, Vol. 135, No. 2, pp. 138–146 (2014).

(8) Q. Yan, B. Zhang, and M. Kezunovic: "Optimization of Electric Vehicle Movement for Efficient Energy Consumption", North American Power Symposium (NAPS), pp. N/A (2014).

(9) T. Guan and C. W. Frey: "Predictive energy efficiency optimization of an electric vehicle using traffic light sequence information*", IEEE International Conference on Vehicular Electronics and Safety, pp. N/A (2016).

(10) X. Wu, X. He, G. Yu, A. Harmandayan and Y. Wang: "Energy-Optimal Speed Control for Electric Vehicles on Signalized Arterials," IEEE Trans. on Intelligent Transportation Systems, Vol.16, No. 5, pp. 2786–2796 (2016).

(11) R. Abousleiman and O. Rawashdeh: "Electric vehicle modelling and energy-efficient routing using particle swarm optimisation", IET Intelligent Transport Systems, Vol.10, No. 2, pp. 65–72 (2016).

(12) O. Nishihara, and S. Higashino: "Energy Conservation Technologies for Electric Vehicles Employing Real-time Optimizations of Lateral and Driving/Braking Force Distributions", Dynamics and Design Conference 2012, pp. N/A (2012) (in Japanese).

(13) Y. Yang, Y. Shih, and J. Chen: "Real-time torque-distribution strategy for a pure electric vehicle with multiple traction motors by particle swarm optimi-

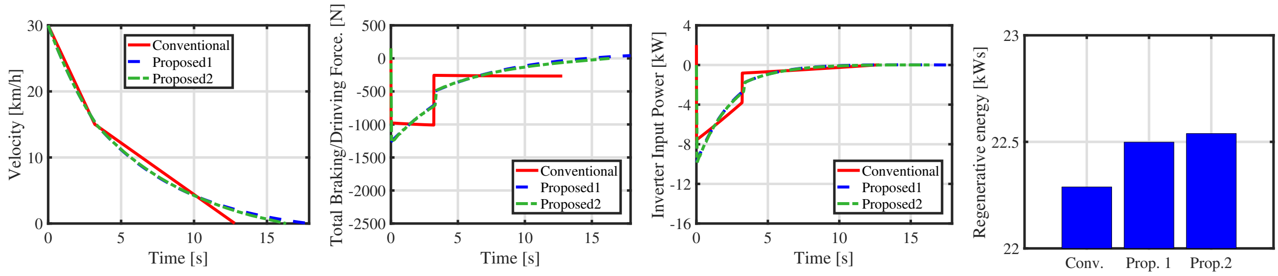

(a) Velocity Trajectory. (b) Total Braking / Driving Force. (c) Inverter Input Power. (d) Regenerative Energy.

Fig. 5. Simulation Results.

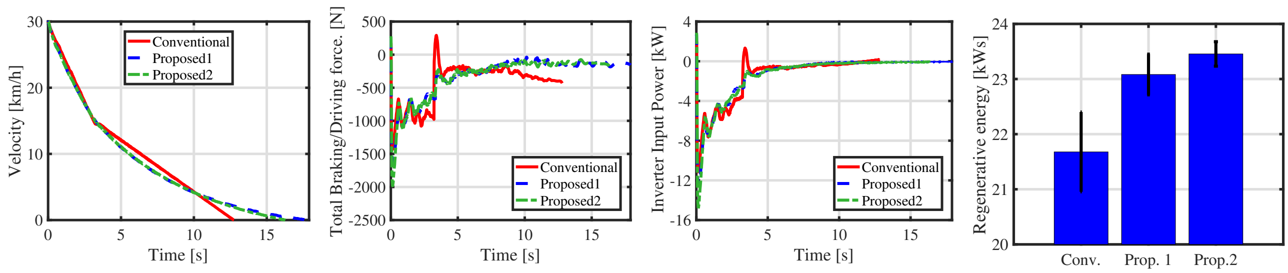

(a) Velocity Trajectory. (b) Total Braking / Driving Force. (c) Inverter Input Power. (d) Regenerative Energy.

Fig. 6. Experimental Results of Field Test.

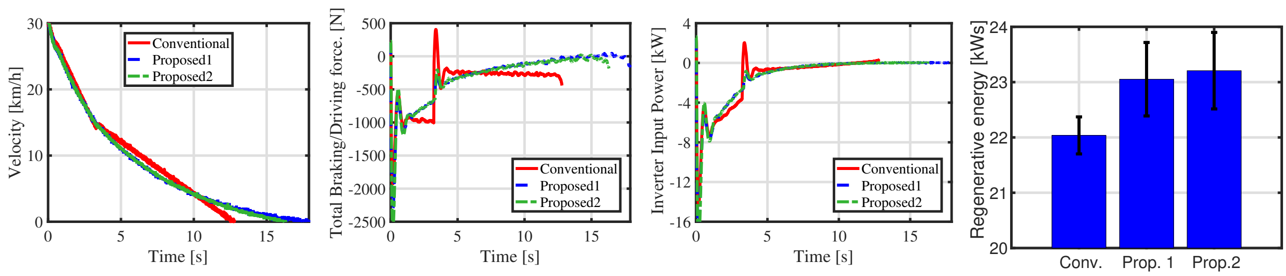

(a) Velocity Trajectory. (b) Total Braking / Driving Force. (c) Inverter Input Power. (d) Regenerative Energy.

Fig. 7. Experimental Results of RC-S.

sation", IET Electrical Systems in Transportation, Vol.6, No. 2, pp. 76–87 (2016).

(14) Y. Chen, X. Li, C. Wiet, and J. Wang: "Energy Management and Driving Strategy for In-Wheel Motor Electric Ground Vehicles With Terrain Profile Preview", IEEE Trans. on Industrial Informatics, Vol. 10, No. 3, pp. 1938–947 (2014).

(15) S. Harada, and H. Fujimoto: "Range Extension Control System Based on Optimization of Acceleration-Deceleration Trajectory and Front and Rear Driving-Braking Force Distribution", SICE 1st Multi-symposium on Control Systems, 6F1-4, pp. N/A (2014) (in Japanese).

(16) H. Fujimoto and S. Harada: "Model–Based Range Extension Control System for Electric Vehicles With Front and Rear Driving–Braking Force Distributions", IEEE Trans. on Industrial Electronics, Vol. 62, No. 5, pp. 3245–3254 (2015).

(17) H. Ko, T. Koseki, M. Miyatake: "Numerical Study on Dynamic Programming Applied to Optimization of Rnning Profile of a Train", IEE of Japan Industry Applications Society Conforence, Vol.3, No. 34, pp.III-271–276 (2004).

(18) D. Kawano, Y. Goto, K. Echigo, and K. Sato: "Analysis of Behavior of Fuel Consumption and Exhaust Emissions under Onroad Driving Conditions Using Real Car Simulation Bench (RC–S)", 2009 JSAE Annual Congress (Spring), Vol. 19, pp. 9–12 (2009) (in Japanese).